Astron. Astrophys. 72, 148—160 (1979)

ASTRONOMY
AND
ASTROPHYSICS

Jupiter's Radiation Belts and Atmosphere

Inke de Pater and Harry A. C. Dames*
Sterrewacht Leiden, Postbus 9513, 2300 RA Leiden, The Netherlands

Received March 1, 1978

Summary. Maps and stripscans of the radio emission from Jupiter were made during the Pioneer 10 flyby in December 1973 at wavelengths 6 cm, 21 cm, and 50 cm using the Westerbork telescope in the Netherlands. With this instrument the disk of the planet was resolved at λ 6 and 21 cm. The pictures are averaged over 15° of Jovian longitude. At 21 cm the stripscans clearly show the existence of a "hot region" in the radiation belts at a longitude $\lambda_{III\,(1965.0)}=255°\pm10°$. Its flux is about 9% of the total non-thermal flux and it has a volume emissivity enhanced by a factor of $\sim$1.6 with respect to the general radiation belts.

The temperature of the thermal disk at 21 cm appears to be 290 ± 20 K. This is likely due to a high ammonia mixing ratio in the atmosphere, a factor of 4–5 larger than the expected solar value of $1.5\,10^{-4}$.

Key words: Jupiter — (non)-thermal emission — hot region — ammonia mixing ratio

1. Introduction

In order to provide a full picture of Jupiter's radiation belts during the Pioneer 10 flyby in December 1973 we mapped the overall distributions of their radio emission at that time using the Westerbork Synthesis Radio Telescope in the Netherlands. Observations were made at all three available frequencies, 610 MHz, 1415 MHz, and 4995 MHz. Due to the low declination of Jupiter at that time (−20°), it was only above the horizon for 7 h per day, and the observations were not as complete or accurate as desired or indeed as possible with the instrument. They do however provide a valuable picture of the overall characteristics of the radiation belts which can be compared with the detailed in situ measurements along the trajectory by the magnetometers (Smith et al., 1974) and particle counters (Simpson et al., 1974; van Allen et al., 1974) to provide a complete picture of the magnetosphere of Jupiter at that time.

2. Observing and Reduction Technique

The properties of the Westerbork telescope and its operation have been described extensively elsewhere (Högbom and Brouw, 1974; Baars and Hooghoudt, 1974; Casse and Muller, 1974; Brouw, 1975). The advantage of using this telescope is the combination of a high resolution with a high sensitivity (see Table 1). This allowed us to divide the data into short intervals and resolve the radiation belts on both sides of the planetary disk averaged over intervals of 15° of Jovian rotation. The observing time consisted of several different sessions of individual durations:

610 MHz (50 cm) − 8 × 1 h (Nov. 3–10, 1973)
1415 MHz (21 cm) − 3 × 7 h (Dec. 5–7, 1973)
4995 MHz (6 cm) − 5 × 7 h + 2 × 5 h (Nov. 20–26, 1973).

After the measurements were corrected for known instrumental and sky effects (van Someren Greve, 1974) they were calibrated by observations of the sources listed in Table 2. The adopted fluxes of 3 C 147, assuming zero polarization for this source, were used to define the gain of the system at all wavelengths (Wilson and Weiler, 1976). The other three sources were used as position calibrators.

The observations at λ 50 cm have been corrected for the Faraday rotation in the Earth's ionosphere using electron density data obtained from the Dutch meteorological institute in De Bilt. At other frequencies this has not been done causing a systematic error of 5° or less in position angle at 21 cm (Weiler and Raimond, 1976) and less than 1° at 6 cm.

Background sources at 21 cm were subtracted using the standard reduction programs. To get rid of these sources at 50 cm all fields at this wavelength were observed twice, once when the planet was in the center of

Send offprint requests to: I. de Pater

* This project was originally planned by Harry Dames. He guided the observations as a start for a Ph. D. project, but soon afterwards he fell fatally ill.

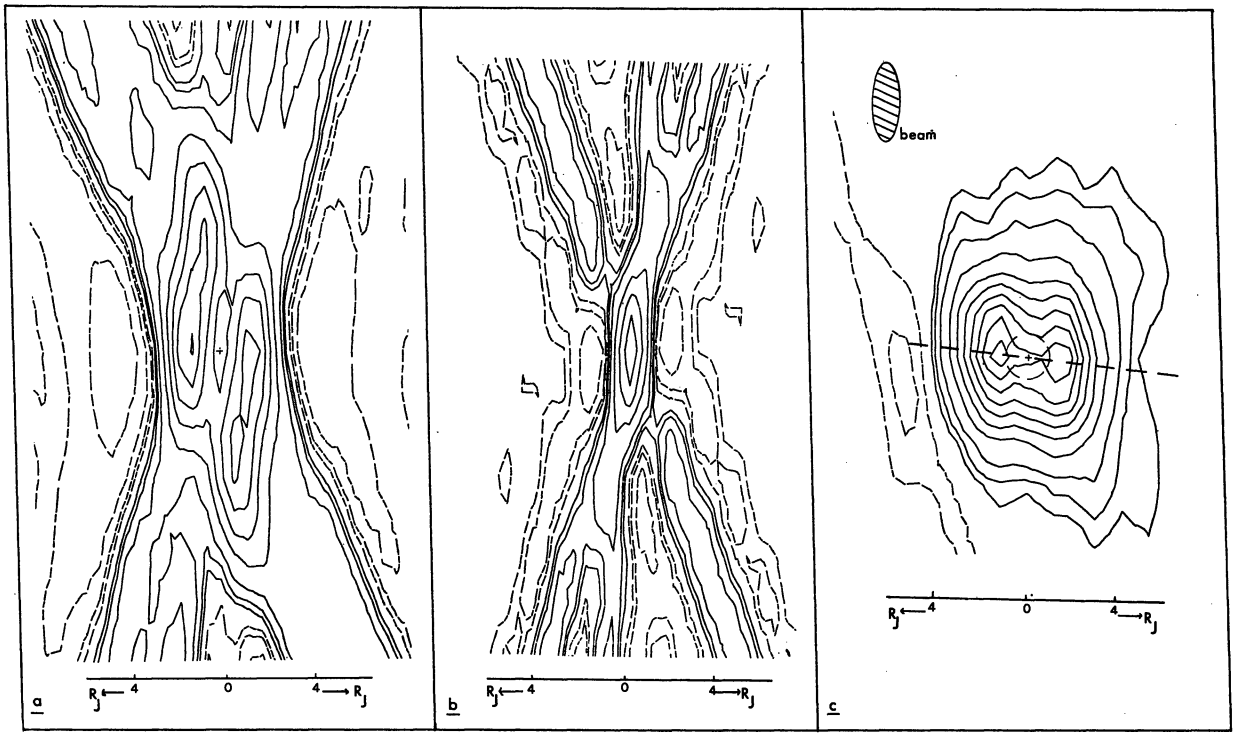

Fig. 1. a A Jovian map at 21 cm, constructed from three short observations at $\lambda_{III}=123°$. The horizontal axis is the distance from the center of the planet in Jovian radii. The contour values in mJy/beam are: 25, 50, 100–1000 (in steps of 100) and similarly for the negative values; these contours are dotted. **b** Pattern of the synthesized beam of the map in **a**. Contour values are 0.05, 0.10, 0.20–1.0 (in steps of 0.20) and even so for the negative values. These values have been chosen to more or less match **a**. **c** The "cleaned" Jovian map from **a**. The planetary disk and the magnetic equator are indicated. The same contour values as in **a** are drawn. The beam area is 4.99 gridpoints; the gridpoint spacing is 9″.89 (=0.55 R_j) in RA and 30″.87 in DEC

Table 1. Telescope performance data

	50 cm 610 MHz	21 cm 1415 MHz	6 cm 4995 MHz	Jovian parameters in Dec. 1973
Resolution or HPBW in RA[a]	54″	22″	6″	Disk: 36″
Field of view[b]	83′	36′	11′	Total extent ~2′.5
Sensitivity (mJy/beam)[c]	1.5	1.5	1.6	Mean flux at 21 cm: 200 mJy beam

[a] Resolution in Dec is $\lambda/L \sin\delta$ radians. For the Jupiter observations it was about 3 times as large as the value in RA
[b] Field of view: the primary beam or HPBW of the individual telescopes.
[c] For a 7 h observation

the field and the second time when the planet was already far out of the field of view. This second observation was subtracted from the first to remove the background sources.

At 6 cm gain variations occurred due to weather and due to instrumental instability. They each could influence the gain of the data by about 10–12%. Corrections were applied which are believed to be good to 5%.

To make pictures of Jupiter at particular rotational aspects we had to remove both the planetary motion along the sky and the rotational motion of the planet from our observations. The first motion could be stopped by moving the phase reference point in the same way that Jupiter moved along the sky. To get rid of the rotational motion we cut the observations at 6 and 21 cm into 25 min pieces which is about 15° in Jovian rotation. This creates a smearing effect on the data which at the angular distance of the radiation belts (the main source of emission at lower frequencies) amount to about 15″; at the planetary surface (the main source of emission at 6 cm), the effect is about 5″. The 50 cm data were only one-hour observations which corresponds to 36° of rotation and gives a smearing of about 36″. We expressed the longitudes belonging to each short observation in Syst. III (1965.0) coordinates (as described in Geoph. Res. Lett. 1977, 4 no 2., p. 65).

Each short observation covers only a very small segment in the plane of spatial frequencies (henceforth called the UV plane). Therefore an observation has a

Table 2. Calibration sources

Source	RA	DEC	Flux[a]		
			6 cm	21 cm	50 cm
3C147	84°68126	49°82858	8.18	21.57	37.78
3C48	23°70761	32°90573	5.80	15.70	28.55
3C309.1	224°73602	71°86977	3.84	8.12	13.51
NRAO 530	262°55614	−13°04609	6.8	5.7	

[a] The fluxes of 3C48, 3C309.1 and NRAO 530 are mean fluxes, derived from the flux of 3C147

resolution mainly in one direction, along the line through the source parallel to the projection of the Westerbork array. At some Jovian longitudes we had more than one observation, each with a different baseline orientation. These were combined to get better coverage of the UV plane and hence better resolution in two dimensions.

Because the distance to Jupiter was continuously changing the total flux received from the planet varied from day to day. To correct to the standard distance of 4.04 AU we multiplied the flux in each interferometer channel by a gain factor $R_{EJ^2}/4.04^2$ where R_{EJ} represents the distance Earth-Jupiter in AU at the time of the observation. Since the angular size of the planet varied maps were made of each observation separately. Before Fourier transforming the data we chose a grid size in RA and DEC such that the spacing of the intensity points on all the final maps would be equal when expressed in Jovian radii.

The 21 cm and 6 cm data had grid-point spacings which were one half and one eigth respectively of the 50 cm spacing. Thus the maps at all frequencies had between 2 and 2.5 points per half power beam width. The maps of the short observations were combined after the Fourier transformation was done which basically gives the same result as Fourier transforming the combined UV points after the appropriate scaling. In this way we could make maps at a few Jovian longitudes at 6 cm and 21 cm. At 50 cm the emission of Jupiter could be resolved only in the right ascension direction. We therefore made stripscans of the planet at this wavelength and also at 21 cm in order to get as much information as possible from the observations. To obtain these scans, the datapoints from each short observation were added such that we got a pure one-dimensional distribution of the source along the line parallel to the projection of the Westerbork array.

One of the maps of Jupiter at 21 cm constructed from three short observations according to the method described above is shown in Fig. 1a. Due to the large unsampled parts of the UV plane the synthesized beam pattern of the telescope is very "dirty" (see Fig. 1b). We removed these effects with help of the procedure "CLEAN", a deconvolution technique developed by Högbom (1974). The maps were restored afterwards

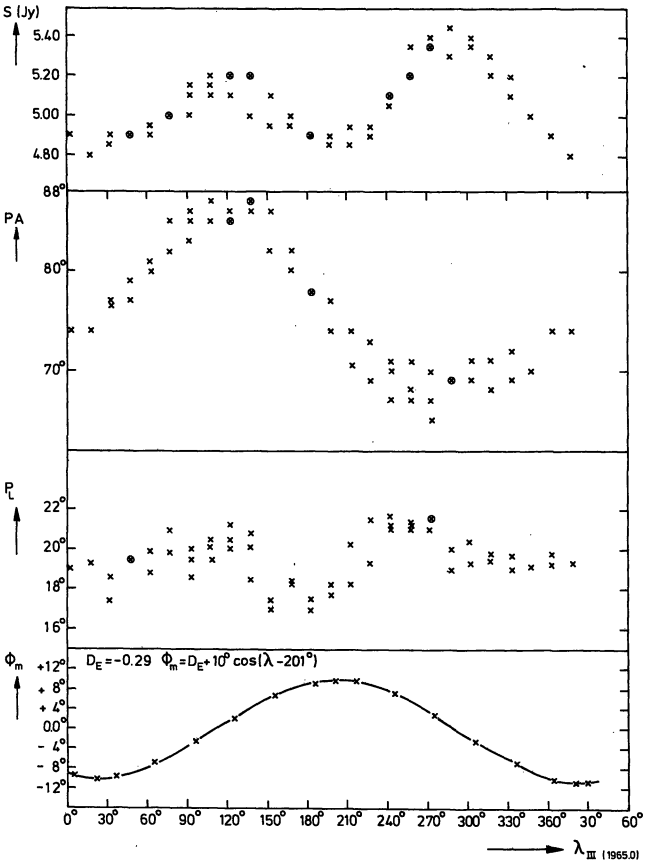

Fig. 2a—d. Various parameters of the integrated radiation of Jupiter at 21 cm as functions of the magnetic longitude of Jupiter (in Syst. III 1965.0). The north magnetic pole is at 201°. **a** Total integrated flux in Jy. **b** Position angle of the electric vector measured eastward from north in the sky. **c** Degree of linear polarization. **d** Magnetic latitude of the Earth with respect to Jupiter

using a Gaussian shaped beam with a half power beam width of 20″.8 which is slightly less (8%) than the synthesized beam width. The result of cleaning the map in Fig. 1a is shown in Fig. 1c. The negative ridge and the shape of the outer contours are clearly due to the deviations of the true antenna pattern from the calculated one. These deviations are somewhat larger than usual as can be expected at such a low declination where the quality of the calibrations is always uncertain. Therefore the uncertainty in this map (and all others) is mainly due to this imperfect beam pattern. The negative ridge along the east side of Jupiter has a mean depth of about 35–40 mJy/beam which is the estimated uncertainty in this beam pattern. The system noise is only a few mJy/beam and the noise in the "cleaned" maps is 20–25 mJy/beam. Adding these quantities quadratically we find a total uncertainty of about 45 mJy/beam in all the 21 cm maps and stripscans. The uncertainty in the maps and stripscans of the polarized flux density is estimated in the same way as being 10–15 mJy/beam, which gives an error of ~3° in the position angles. The instrumental polarization is ~0.5% (Weiler, 1973)

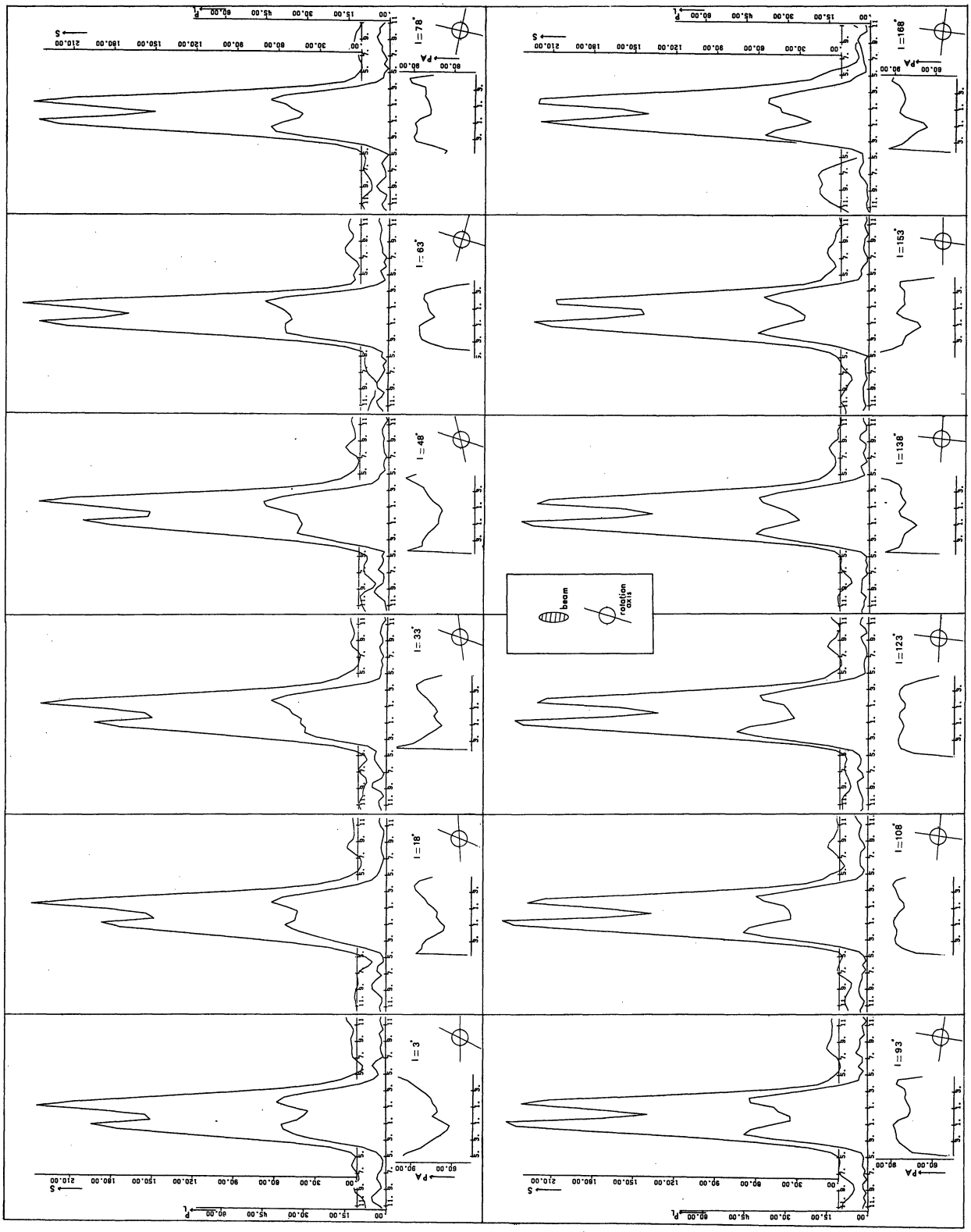

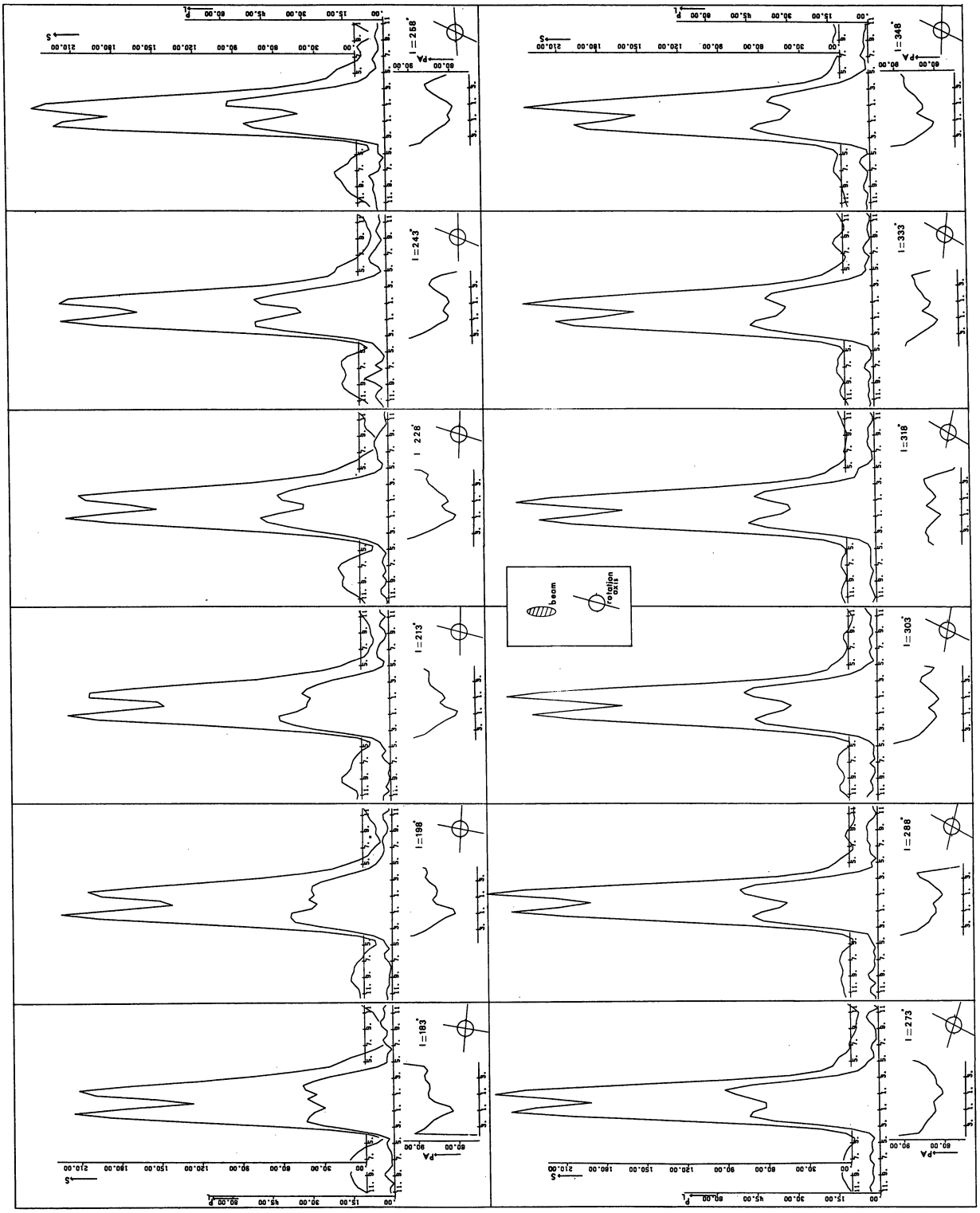

Fig. 3a and b. Stripscans at 21 cm: each scan is averaged over 15° of Jovian longitude. Indicated are the non-thermal flux density, polarized flux density and the position angle of the electric vector. The flux densities are expressed in units of 5 mJy/beam. The beam width has a mean value of 2.30 gridpoints. This width varies by a maximum of 0.4% due to the different projected baseline lengths and unequal gridpoint spacings (0.55 R_J; see also Sect. 2). The horizontal axis is the distance from the center of the planet in Jovian radii. In the lower right hand corner of each plot the direction of the magnetic axis is indicated by the approximately vertical line and the direction along which the stripscan was taken by the approximately horizontal line. Note that the beam indicated should really be a fan beam

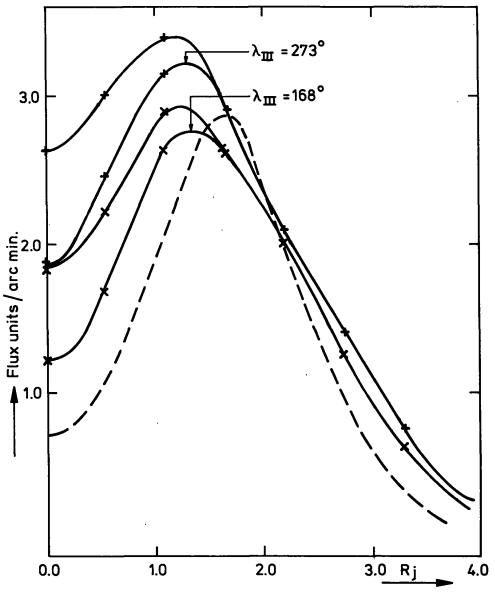

Fig. 4. Comparison of Berge's (1966) 10.4 cm scan represented by a dotted line (he subtracted a thermal disk of 260 K) with two one-dimensional distributions from Fig. 3, at $\lambda_{III}=273°$ and $\lambda_{III}=168°$. The solid upper curves correspond to the total flux with a 236 K disk subtracted; the lower curves have a 387 K disk subtracted. For more details, see the text

which is only a few mJy/beam. At 6 cm we have an additional error in the gain due to the instability of the system and the weather as was mentioned above. This error is about 5% which is 60 mJy/beam for the maximum intensity. The noise due to amplitude and phase errors is 25–30 mJy/beam. The total uncertainty in the 6 cm maps appears to be about 70 mJy/beam.

3. Results

3.1 Integrated Jovian Parameters

Figure 2 shows various parameters of the integrated Jovian radiation as functions of the magnetic longitude (Syst. III 1965.0), averaged over 15° intervals. At each longitude the emission is observed with 20 interferometers, pairs of different baselines and the integrated quantities were calculated directly from the receiver outputs by extrapolating these values as a function of baseline length to zero baseline. Fig. 2 shows:

a) Total integrated flux density in Jy referred to 4.04 AU.

b) The position angle of the electric vector measured eastward from the north on the sky. Because of the rotational pole of Jupiter was inclined from north by 342°.7 the mean position angle of the electric vector is centered around 76°.7 rather than around 90°.

c) Degree of linear polarization.

d) Magnetic latitude of the Earth with respect to Jupiter. This latitude, ϕ_m, was calculated according to the relation $\phi_m = D_E + \beta \cos(\lambda_{III} - \lambda_0)$ (Berge and Gulkis, 1976). D_E is the declination of the Earth relative to Jupiter's rotational equator (−0°.29 at this epoch), β is the angle between Jupiter's magnetic and rotational axes taken as 10° and λ_0 is the central meridian longitude of the north magnetic pole taken as 201° (Syst. III 1965.0). The variations with longitude are consistent with the beaming found by others from the integrated data (Berge and Gulkis, 1976; Gardner and Whiteoak, 1977; Neidhöfer et al., 1977). Moreover the figure shows two anomalies: 1. a deviation from a sine curve of the position angle at longitude larger than 200°. This has already been found and interpreted by Conway and Stannard (1972) using Branson's maps (1968). They suggested that these deviations are due to a sort of "hot spot" near longitude 200°. 2. a difference in height of the two flux density maxima, much more pronounced than has ever been detected before (see i.e. Berge and Gulkis, 1976). In the next section it will be clear that this likely is due to the existence of a hot region at a longitude of ~255°.

3.2 One Dimensional Stripscans

21 cm

Figure 3 shows stripscans of the planet at 21 cm at 24 different rotational aspects averaged over 15°. The figure shows the non-thermal flux (with a thermal disk of 236 K subtracted, see below), the linear polarized flux, and the position angle of the electric vector (defined as in Fig. 2). In the lower right hand corner of each plot the direction of the magnetic axis is indicated by the approximately vertical line and the direction of the stripscan by the approximately horizontal line. There is a clear variation in longitude of the amount of flux we receive from both sides of the disk and from these data we would estimate the existence of a hot region at a longitude of 255° ± 10°. The width of the profile outlining the emission region also shows a small change corresponding to the hot region. It appears to be smallest at the longitude of the hot region and largest 90° away from it. If we assume a ringlike structure for the radiation belt (as shown in the top view of Fig. 8) with an imbedded hot region the above data can be used to give rough estimates of the flux and size of this region. From the difference in flux densities received from both sides of the belt and the difference in the maxima of the total flux density in Fig. 2 the flux of this hot region is estimated to be about 0.4 Jy out of a total of about 4.5 Jy. With the additional information of the change in width of the emission region the extent is estimated to be about 50° in longitude which means that its volume emissivity is enhanced by a factor of about 1.6 with respect to the general radiation belts.

Branson's maps (1968) showed the hot region at a longitude of about 190° (Syst. III 1965.0) while our data

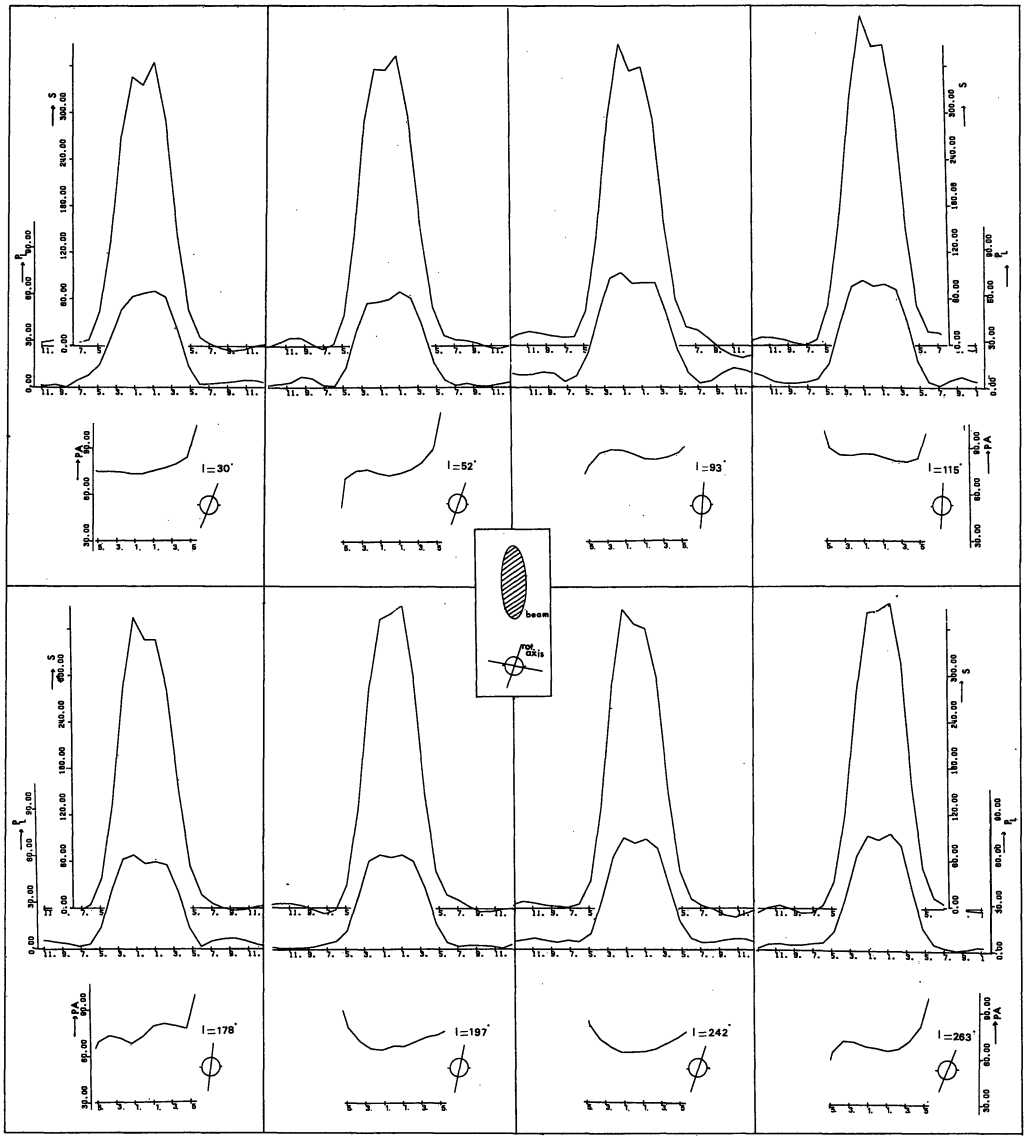

Fig. 5. Stripscans at 50 cm. In the middle of the figure the rotational axis is indicated together with the direction along which the source is resolved by the approximately horizontal line. See also the caption to Fig. 3

place it at 250°–260°. Although Branson's maps are averaged over 120° of longitude an error of about 60° is not very likely. Possibly this region moves or has moved through the belt. More observations are needed to clarify this problem.

Figure 4 shows a comparison of two one-dimensional distributions with Berge's 10.4 cm scan (1966). Berge's scan is obtained by adding both polarized components observed (P.A. = 0° and P.A. = 90°; see Berge and Gulkis, 1976). Our own scans were obtained by folding the East half over the West half and averaging the curves. The upper (solid) curves correspond to the total flux density with the emission from a thermal disk at 236 K subtracted, the lower curves have a thermal disk of 387 K subtracted. The general shape of the radiation belts does not show any significant dependence upon the amount of thermal flux subtracted. The distance from the center of the disk to the peaks in the emission of the belts is about 0.3 R_j smaller than found in Berge's scan. This shift is similar to the shift seen in Olsen's 3.7 cm and 11 cm data (Berge and Gulkis, 1976). From many Jovian observations in the past 10 yr we know that its flux decreased suddenly at all frequencies in the year 1972 (Klein, 1975; Hide and Stannard, 1976). The low mean total flux of 5.1 Jy detected here with Westerbork is in agreement with this. Maybe there is a relation between this sudden decrease in flux and the inward displacement of the belts. (I thank E. T. Olsen for this suggestion).

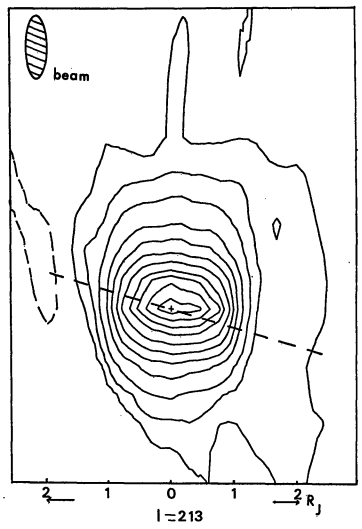

Fig. 6. Map of the total intensity at 6 cm at a longitude $\lambda_{III}=213°$. Contour values in mJy/beam: 35, 75, 150–900 (in steps of 150), 1000–1200 (in steps of 100). The negative contours are dotted; the beam width is 6.30 gridpoints. The gridpoint spacing is 2".57 ($\approx 0.14\ R_j$) in RA and7".75 in Dec.

50 cm

Figure 5 shows the stripscans at 50 cm obtained in the same way as the 21 cm scans. The errors are about equal to those in the 21 cm scans. The flux density also shows the sinuoidal variation with longitude (see Table 3). As far as we can distinguish the two sides of the radiation belt, the existence of a hot region at a longitude 250°–260° is not in disagreement with these data. These scans are mainly useful in comparing the data at the three different wavelengths. Convolving the 6 cm and 21 cm scans to the resolution of the 50 cm data we increased the gridspacing by factors of 8 and 2 respectively. At 6 cm we subtracted a thermal disk of 236 K, at 21 cm of 290 K, the temperatures deduced from two dimensional maps (see below). At 50 cm a thermal flux of 0.1 Jy was subtracted corresponding to a temperature of ~265 K. The width of the emission region R_e (half power width) at 6 cm is $97'' \pm 5''$, at 21 cm $108'' \pm 5''$ and at 50 cm $117'' \pm 5''$. It appears that R_e increases with wavelength roughly as $R_e \sim \nu^{-0.1}$. This indicates that the lower energy particles which radiate at longer wavelengths (in a dipole-like configuration with sizes as measured at the various wavelengths) have mean orbital distances farther from the center than the higher energy electrons. This is similar to the situation found for the Earth's radiation belts (Søraas, 1973).

The ratio of the degrees of the integrated linear polarization at 50 cm to 21 cm (after convolution) is 0.9 ± 0.15. The integrated position angles of the electric vectors are about equal at both wavelengths and hence depolarization and Faraday rotation are both undetectable in the source. The spectral index of the synchrotron component (defined such that $S_\nu = \text{const}\ \nu^{-\alpha}$) of the integrated emission between 21 cm and 50 cm appears to be about $\alpha = 0.08 \pm 0.05$ which implies a mean energy spectrum of electrons in this range of

$$N(E)dE \sim E^{-1.16}\,dE.$$

The non-thermal flux at 6 cm had such a large error (20–30%) that we did not use this flux in the spectral index calculation.

Table 3. Total flux at 50 cm

Mean longitude in degrees	Total flux in Jy
30	4.39
52	4.51
93	4.72
115	4.94
178	4.46
197	4.60
242	4.58
263	4.66

3.3 Two Dimensional Pictures

6 cm

Figure 6 shows one of the five maps we got at 6 cm. They all show the planet clearly resolved in the E.W. direction and they are quite similar in appearance. This probably means that there are no longitude dependent features on the disk with a deviation in intensity more than about 8% of the maximum, a value which is estimated from the 70 mJy/beam uncertainty in the maps. The apparent limb-darkening in the declination direction is probably not real. The weather was so bad during the period of the 6 cm observations it is likely that the atmospheric extinction was larger than assumed in the reduction program. With the synthesis interferometer, the data giving the north-south discrimination in the source were obtained when Jupiter was near the horizon at large hour angles where the extinction correction was most serious. If the extinction is larger than assumed the polar intensities will be reduced.

The radiation belts outside the thermal emission region do not appear in Fig. 6 as they are just below the noise level.

Figure 7 shows a cut through the planet in the E.W. direction after subtraction of non-thermal radiation approximated by a model with a peak intensity of 90 mJy/beam at a distance larger than 1.4 R_j and decreasing to 36 mJy/beam in front of the planet. This model then was convolved with the proper beam. As a comparison we modelled the thermal emission of the planet by a uniform oblate disk filled with volume elements of $2''.5 \times 2''.5$ and the disk was then convolved with the proper beam. The upper curve in Fig. 7 shows

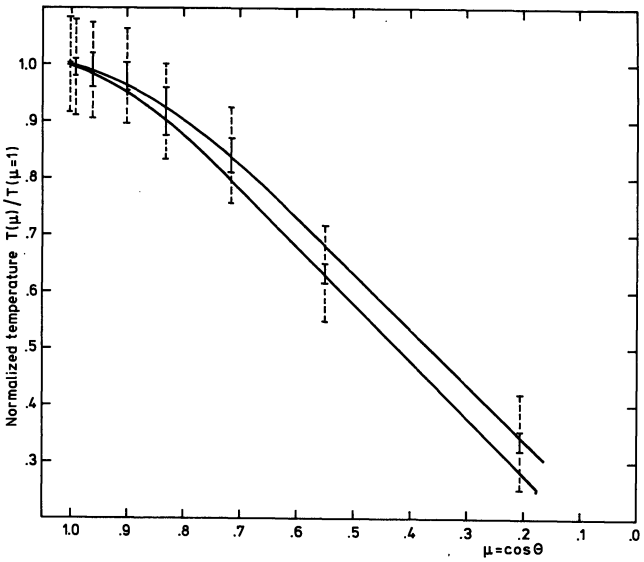

Fig. 7. A cut through the planet at 6 cm. The parameter $\mu=\cos\theta$ is indicated on the horizontal axis. θ is the angle a ray makes with the vertical to the atmosphere. On the vertical axis the normalized temperature $T(\mu)/T(\mu=1)$ is indicated. The two curves drawn represent models of the oblate disk with (the lower curve) and without (upper curve) limb darkening taken into account (according to Berge and Gulkis, 1976). For more details the reader is referred to the text. The vertical solid lines indicate the range of temperatures shown by the five Westerbork maps, the dotted lines are a measure of the error in each of these maps; they are drawn starting at the middle of the solid lines

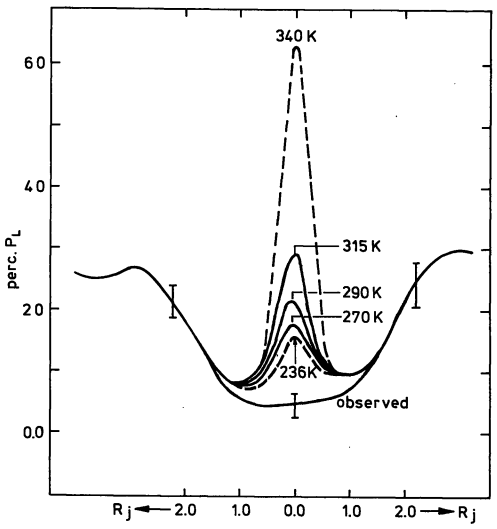

Fig. 9. The degree of linear polarization in the equatorial plane of Jupiter at 21 cm, $\lambda_{III}=108°$. The horizontal axis is the distance from the center of the planet in Jovian radii. The lowest curve gives the observed degree of polarization of the total radiation received from the planet. The other curves show the polarization after subtraction of various disks: 236 K, 270 K, 290 K, 315 K, and 340 K. A few errorbars are indicated. In order to obtain the same fractional polarization in the central ray as in a ray passing through the outer parts of the radiation belt the disk temperature must be 290 ± 20 K

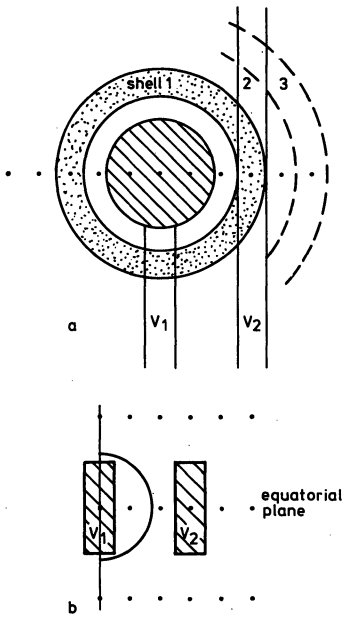

Fig. 8. **a** Top view of the model of Jupiter's radiation belts. **b** Observer's view of the model of Jupiter's radiation belts. The dots represent its matrix of datapoints on the Westerbork map at 21 cm with the size of the Jovian disk indicated by the thick line. The belts are modelled by three cylindrical shells as indicated in **a**. Each shell has a thickness of 1 gridpoint. Integration over the rectangles V_1 and V_2 along the line of sight gives the vloume emissivity at the gridpoint in the center of the rectangle

the predicted temperature curve in the E.W. direction. Then the disk was limb darkened according to the theoretical curve of Berge and Gulkis (1976) for an ammonia mixing ratio in Jupiter's atmosphere of $1.5\,10^{-4}$ and convolved with the beam to give the lower curve in Fig. 7. An increase in the ammonia mixing ratio will reduce the apparent limb darkening moving the curve closer to that of the non limb darkened case. As was to be expected the measurements are rather insensitive to limb darkening but there is a slight tendency toward less limb darkening than expected from the curve of Berge and Gulkis (1976).

The thermal disk temperature at 6 cm was estimated from all five maps to be 236 ± 15 K which corresponds to a flux of 7.4 ± 0.4 Jy. The quoted error is that of any individual map. The temperature was determined simply by integrating the flux inside the 75 mJy/beam contour and subtracting from it an estimated non-thermal contribution equal to 60 mJy/beam outside the visible disk and one-half of this amount in front of the disk.

21 cm

In Fig. 1 a picture of the total radiation received from Jupiter was shown. In order to make pictures of only the non-thermal radiation we have to separate both components of the emission. Estimated values for the temperature of the disk at 21 cm range from a temper-

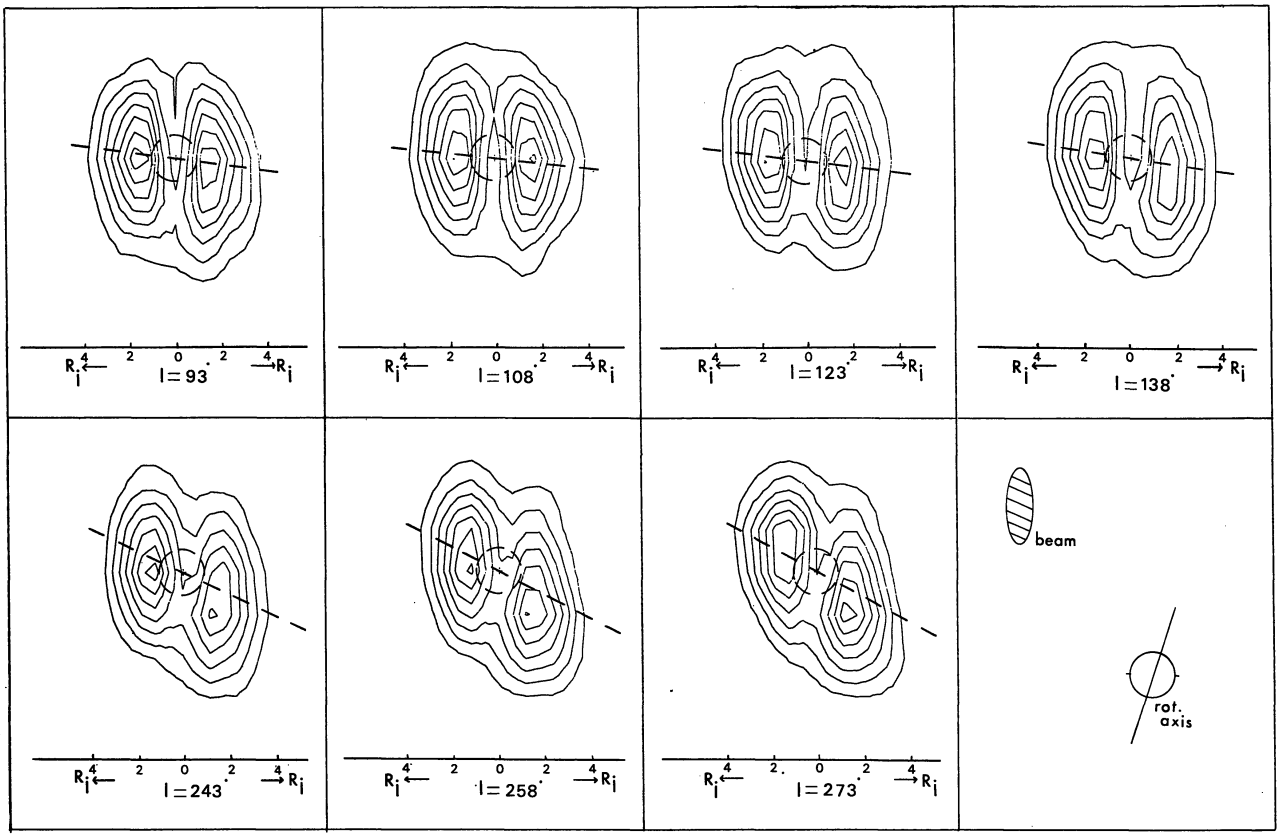

Fig. 10. Maps of the non-thermal emission at 21 cm from Jupiter's radiation belts. A thermal disk of 290 K has been subtracted from the total radiation received. Contour values in mJy/beam: 150–1050 in steps of 100. The beam area is 4.99 points. The gridpoint spacing is 9.″89 (= 0.55 R_j) in RA and 30.″87 in DEC. The various longitudes are indicated in Syst. III (1965.0). The magnetic equator and the planetary disk are sketched in the pictures by dotted lines. On the horizontal axis is the distance from the center of the planet in Jovian radii

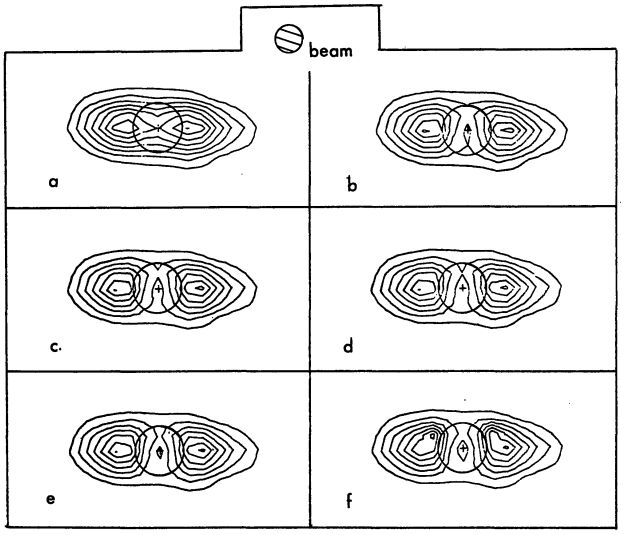

Figs. 11a—f. Maps of the Jovian radiation at 21 cm, $\lambda_{III} = 108°$ with the plotscale in declination decreased by a factor of sin δ with respect to right ascension. **a** total radiation, **b—f** the emission with thermal disks of 236 K, 270 K, 290 K, 315 K, and 340 K respectively subtracted. Note that the planetary disk indicated should really be flattened by a factor sin δ in declination

ature of 236 K as found at 6 cm to ~400 K as predicted by the theoretical curve of Gulkis (1973) for a convective model atmosphere with solar abundances of all chemical elements. Branson (1968), who first determined the thermal disk temperature at this wavelength from observations, deduced a temperature of 250 ± 40 K. However his determination has some shortcomings:

a) the map he used was averaged over 120° of Jovian longitude,

b) the hot spot in this map was moving from the left side of the planetary disk towards the right passing the planet in front of it,

c) he assumed negligible radiation originating above or below the planetary disk which certainly will be present as appears from the present Westerbork maps (see below), and

d) he assumed a flux-density for the non-thermal radiation just in front of the planet to be one-half that received outside the limbs, while a factor of one-third would be more realistic.

Point d) would end up in a too low disk temperature but the first three ponts will partly compensate for this effect.

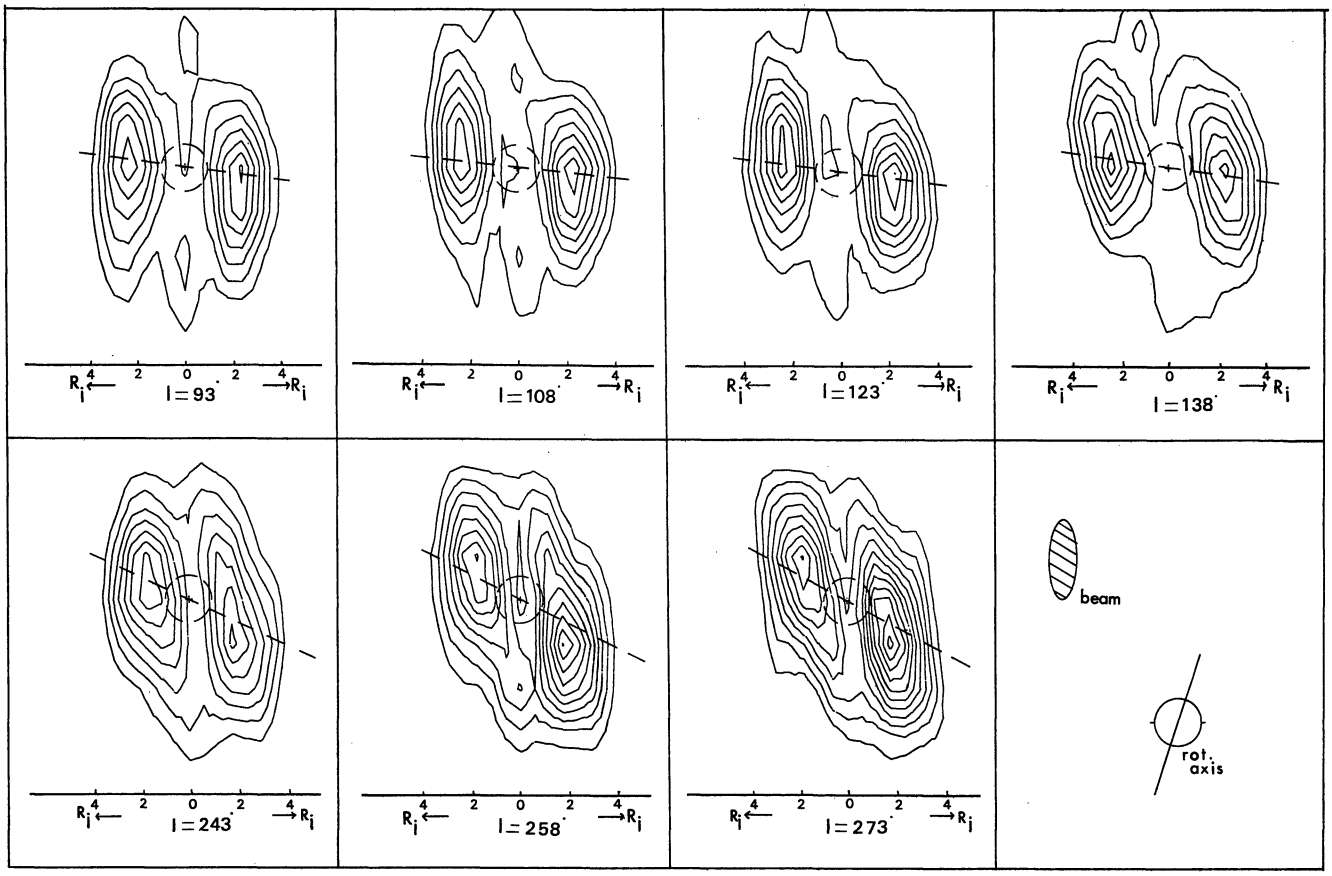

Fig. 12. Polarized flux density $(Q^2+U^2)^{1/2}$ of the maps in Fig. 10. Contour values in mJy/beam: 35–200 in steps of 15

To determine a more accurate temperature at this wavelength we compared the observed variation of both the total intensity and the degree of linear polarization across the equatorial plane of Jupiter with values calculated for different models. With both methods we used maps where we see the magnetic equator roughly edge-on and the hot region is on the far side of the planet.

The total intensity of the radiation belts was modelled by a series of uniform isotropic cylinders circling the planet as shown in the top view in Fig. 8a with the dimensions shown in Fig. 8b. The integrated brightness along the line of sight at the peaks of the radiation belts and at the center of the disk were then evaluated and compared with the observed values after subtraction of disks with various brightness temperatures. Using this method on the stripscans seen in Figs. 3 and 4 gives a disk temperature of 360 K.

The observations show considerable emission over the poles of Jupiter which is in contradiction with previous observations (Roberts, 1976). There are admittedly phase errors in the Jovian data which can be interpreted as positional errors of $\sim 10''$ in the declination direction (this larger error arises from the fact that the maps are constructed with only three very small segments in the UV plane being filled) and which will smear out radiation towards the poles of Jupiter. Even after a correction for this effect has been applied the maps still indicate considerably more emission originating from over the poles than found by Roberts (1976). When this extra polar emission is taken into account, the disk temperature is less than 360 K found above and cannot be greater than ~ 300 K. Because of all the assumptions this method is not very precise, however.

Figure 9 shows the degree of linear polarization in the equatorial plane of the two-dimensional maps after subtraction of thermal disk models of various temperatures. In order to obtain the same fractional polarization in the central ray as in a ray passing through the outer parts of the radiation belt, we must have a disk temperature of 290 ± 20 K. This determination is much more precise than the method involving the brightness distribution.

It is clear that the disk temperature, 290 ± 20 K, is at least ~ 100 K lower than the theoretically estimated value of Gulkis (1973). We have tried to interpret this fact in terms of changes in atmospheric structure, such as the existence of a large amount of H_2O or a strong obscuration by NH_4SH, or an increase with respect to the solar value in the mixing ratio of NH_3, the gas which provides the strongest radio opacity in the Jovian

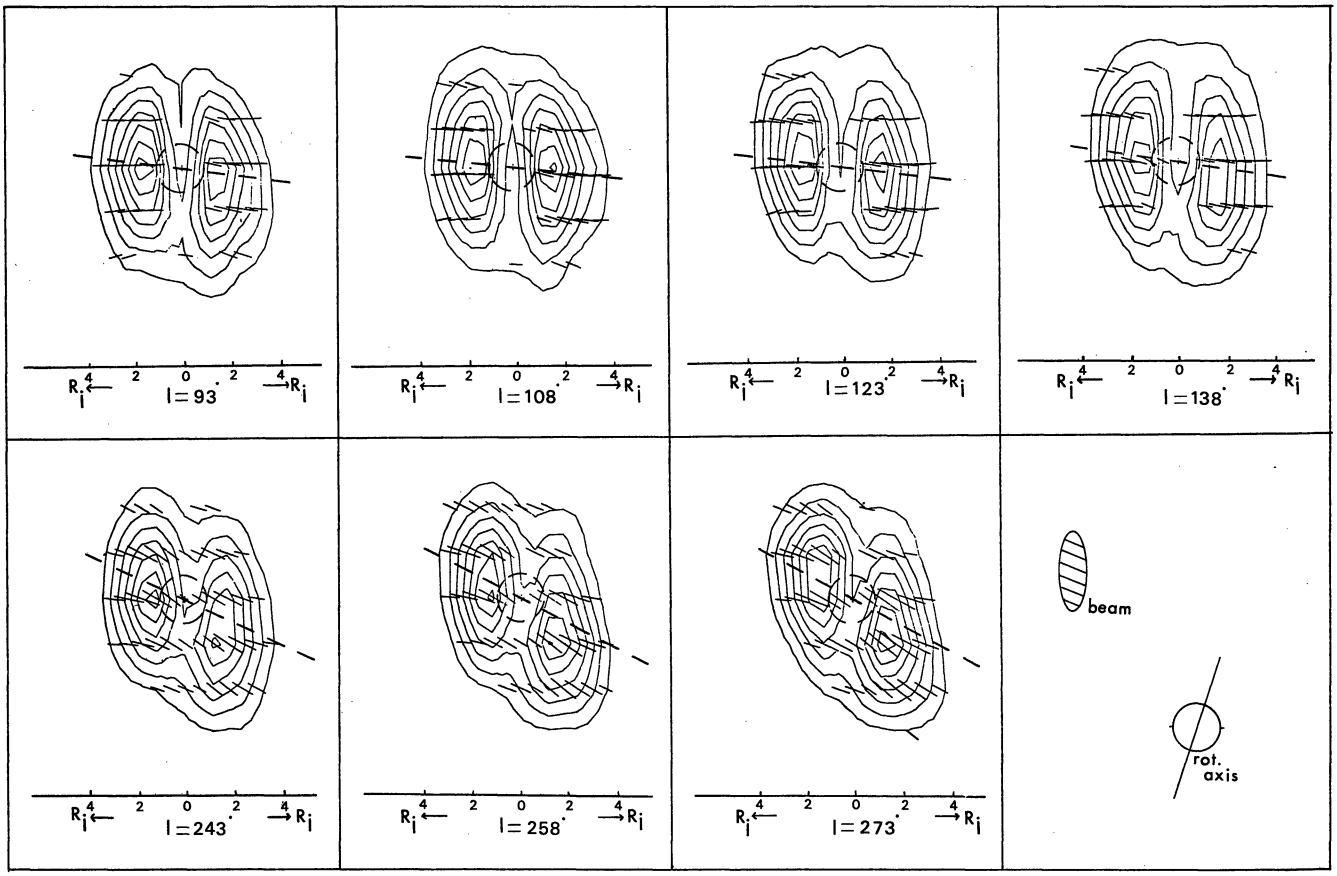

Fig. 13. Position angles of the electric vectors at 21 cm superimposed on the intensity maps from Fig. 10. The angles are measured eastward from the north in the sky. The length of these vectors is a measure of the intensity of the polarized flux from Fig. 12

atmosphere. The existence of a kind of a physical (solid) surface at temperatures as high as 270–300 K and pressures less than 10 atm is a very unrealistic model (Goodman, 1969). Infrared measurements at 5 μ shows that the mixing ratio of water certainly is less than $\sim 10^{-5}$ (Larson et al., 1975). To raise this mixing ratio would require sinks of water ice or droplets in which case an aqueous ammonia solution should exist (assuming a uniform distribution of the droplets or water ice) so that the mixing ratio of ammonia would need to become $\sim 10^3$ times the solar ratio which is much too high for the observations at shorter wavelengths. According to theoretical atmospheric models of Lewis (1969) a NH_4SH layer may exist beneath the NH_3 clouds. However we do not expect a noticeable absorption by such a layer since then the cloud has to be very thick which, based upon the same arguments as given above, is not likely. According to the theoretical temperature—versus—wavelength curves of Gulkis (1973) a temperature $T_D \approx 290$ K is consistent with an ammonia mixing ratio of $6-8\ 10^{-4}$, a factor of 4–5 above the solar value. This factor is about equal to the factor by which Wallace and Hunten (1977) increased their mixing ratio of CH_4 in the region 0.4–1.1 μ. Together with the depletion of oxygen by a factor >100 compared with the solar value these abundances will be very interesting for future work.

The maps of the non-thermal emission of Jupiter after subtraction of a thermal disk model of 290 K are shown in Fig. 10. The uncertainty in the maps is ~45 mJy/beam as has been said in Sect. 2. The southward shift of the radiation belts seen in the lower three pictures is probably not real, but due to phase errors in the short observations (see above in the discussion concerning emission from above the poles). Squeezing the plotscale from Fig. 10 in declination by a factor sin δ relative to the scale in right ascension will give the appearance of the maps having been made with a circular beam. Any non-circularity then is due to a true extension of the radiating region in that diection. According to Berge's (1966) model we would expect an extent in declination of about 30″ for the radiation belts (at the half power level). With a beam extent of ~70″ in that direction we do not expect to resolve the belts in the N-S direction. Figure 11 shows the results for $\lambda_{III} = 108°$. Part *a* is the total radiation map, *b–f* are the maps with a thermal disk of 236 K, 270 K, 290 K, 315 K, and 340 K respectively subtracted. There is clearly an extension of the belts in the right ascension direction in

agreement with Berge's model. The pictures b—e also show that there is only a slight difference between subtraction of a thermal disk of 236 K or of 315 K. Here again as in the stripscans the distance between the peaks of the belts is smaller than in Berge's model.

Figure 12 shows the polarized flux density $(Q^2+U^2)^{1/2}$ and Fig. 13 the position angles of the electric vector superimposed on the intensity maps of Fig. 10. The length of these vectors is a measure of the intensity of the polarized flux. These angles all appear reasonably parallel on the two sides of the planet. To get information on the magnitude of any magnetic anomaly associated with the hot region we need more sensitive data, intended to achieve with further observations in 1978.

Conclusions

The main results from this work are the following:

Thermal Radiation

a) The thermal disk of Jupiter measured at a wavelength of 6 cm has a temperature of 236 ± 15 K.

b) There may be some limb darkening over the planetary disk at 6 cm.

c) The temperature of the thermal disk at 21 cm appears to be 290 ± 20 K.

d) The ammonia mixing ratio may be a factor of 4–5 larger than the solar value of $1.5\ 10^{-4}$.

Non-thermal Radiation

e) The radiation belts have an overall structure governed by the trapping of electrons in the dipolar field of the planet with significant beaming of the synchrotron radiation into the plane of the magnetic equator.

f) The total flux received is less than the fluxes received a few years earlier, but in agreement with the level obtaining after the sudden decrease in flux in 1972.

g) A comparison of our scans with Berge's 10.4 cm scan observed prior to 1972 showed a decrease in the distance from the disk center to the flux peaks.

h) There exists a hot region in the radiation belts with

1. a position of λ_{III} $(1965.0)=255°\pm10°$,

2. a flux of 0.4 Jy which is 9% of the total non-thermal flux,

3. an extent of about 50° in longitude and a volume emissivity enhanced by a factor of ~1.6 with respect to the general radiation belts,

4. the position of this hot region may be drifting with time.

i) The lower frequency (longer wavelength) emision comes from further out in the radiation belts implying that the lower energy particles are farther away from the center (assuming a dipole-like configuration with sizes as measured at the various frequencies).

j) The spectral index of the integrated synchrotron radiation between 21 cm and 50 cm is $+0.08\pm0.05$.

Acknowledgements. Valuable suggestions and comments concerning the interpretation of the data from J. R. Dickel are gratefully acknowledged. (He is supported in part by NASA Grant NGR-14-005-176.)

I also want to express my thanks to R. S. le Poole for his advice and continued encouragement, to H. van der Laan for his continuous interest and his initiative in acquiring NASA support for this research.

I thank the Westerbork telescope and reduction groups for their careful help in the data observation and reduction, especially H. W. van Someren Gréve. The Westerbork Radio Observatory is operated by the Netherlands Foundation for Radio Astronomy with the financial support of the Netherlands Organization for the Advancement of Pure Research (Z.W.O.). This research was supported by National Aeronautics and Space Administration, Grant NSG-7264.

References

van Allen, J.A. et al.: 1974, *J. Geoph. Res.* **79**, p. 3559
Special issue concerning the Pioneer 10 mission
Baars, J.W.M., Hooghoudt, B.G.: 1974, *Astron. Astrophys.* **31**, 323
Beard, D.B., Luthey, J.L.: 1973, *Astrophys. J.* **183**, 679
Berge, G.L.: 1966, *Astrophys. J.* **146**, 767
Berge, G.L., Gulkis, S.: 1976, in Jupiter, p. 655. Ed. T. Gehrels, University of Arizona Press, Tucson, Arizona
Branson, N.J.B.A.: 1968, *Monthly Notices Roy. Astron. Soc.* **139**, 155
Brouw, W.N.: 1971, Ph. D. dissertation. University of Leiden, The Netherlands
Brouw, W.N.: 1975, *Methods in Comput. Phys.* **14**, 131
Casse, J.L., Muller, C.A.: 1974, *Astron. Astrophys.* **31**, 333
Conway, R.G., Stannard, D.: 1972, *Nature Phys. Sci.* **239**, 142
Gardner, F.F., Whiteoak, J.B.: 1977, *Astron. Astrophys.* **60**, 369
Goodman, G.C.: 1969, Ph. D. dissertation. University of Illinois. Urbana, Illinois
Gulkis, S.: 1973, *Space Sci. Rev.* **14**, 497
Hide, R., Stannard, D.: 1976, in Jupiter, p. 767. Ed. T. Gehrels, University of Arizona Press, Tucson, Arizona
Högbom, J.A.: 1974, *Astron. Astrophys. Suppl.* **15**, 417
Högbom, J.A., Brouw, W.N.: 1974, *Astron. Astrophys.* **33**, 289
Klein, M.J.: 1975, *Nature* **253**, 102
Larson, H.P., Fink, U., Treffers, R., Gathier III, T.N.: 1975, *Astrophys. J.* **197**, L 137
Lewis, J.A.: 1969, *Icarus* **10**, 365
Luthey, J.L., Beard, D.B.: 1973, *Astrophys. J.* **183**, 671
Neidhöfer, J., Booth, R.S., Morris, D., Wilson, W., Biraud, F., Ribes, J.C.: 1977, *Astron. Astrophys.* **61**, 321
Roberts, J.A.: 1976, *Proc. Astron. Soc. Australian* **3**, 53
Simpson, J.A. et al.: 1974, *J. Geoph. Res.* **79**, p. 3522
Special issue concerning the Pioneer 10 mission
Smith E.J. et al.: 1974, *J, Geoph. Res.* **79**, p. 3501
Special issue concerning the Pioneer 10 mission
Van Someren Greve, H.W.: 1974, *Astron. Astrophys. Suppl.* **15**, 343
Søraas, F.: 1973, in Cosmical Geophysics, ed. A. Egeland, Ø. Holter and A. Omholt. Universitetsforlaget, Oslo-Bergen-Tromsö
Wallace, L., Hunten, D.M.: 1977, *Rev. Geophys. Space Phys.* (in press)
Weiler, K.W.: 1973, *Astron. Astrophys.* **26**, 403
Weiler, K.W., Raimond, E.: 1976, *Astron. Astrophys.* **52**, 397
Wilson, A.S., Weiler, K.W.: 1976, *Astron. Astrophys.* **49**, 357